Biointerface Research in Applied Chemistry
Open-Access Journal (ISSN: 2069-5837)

Article
Volume 14, Issue 3, 2024, 74
https://doi.org/10.33263/BRIAC143.074

In Silico Analysis of Astaxanthin and Ellagic Acid as Inhibitors of UV Induced MAPK Pathway in Melanoma Carcinogenesis

Vaishnavi Bose Subash Chandra Bose [1], Vidhyabharathi Balaganesan [1], Gayathri Govindaraj [1], Veerabhuvaneshwari Veerichetty [1,*]

[1] Department of Biotechnology, Kumaraguru College of Technology, Coimbatore – 641049, India
* Correspondence: veerabhuvaneshwari.v.bt@kct.ac.in;

Scopus Author ID 57204479160
Received: 29.04.2023; Accepted: 28.05.2023; Published: 17.02.2024

Abstract: Prolonged exposure to UV radiation activates the protein kinases and leads to photoaging, cell damage, DNA damage, and skin cancers. These effects can be reduced when the activation of these protein kinases is inhibited. *In silico* studies are carried out to test the potential of Astaxanthin and ellagic acid in inhibiting the UV-mediated melanoma carcinogenesis pathway. The protein kinase targets of UV-induced MAPK pathway are selected and docked with Astaxanthin and ellagic acid using AutoDock Vina software. These results will be compared with two standard drugs, Luteolin and Taxifolin, following the same docking procedures. The binding energies of Astaxanthin and ellagic are compared with standard drugs. With certain specific protein kinase targets, both astaxanthin and ellagic acid showed greater affinity than the standard drugs, while in some cases, ellagic acid alone showed greater affinity, and in others, the affinity was less than equal to the standard drugs. The inhibition constant values of Astaxanthin and ellagic acid are like that of standard drugs. This study confirms that Astaxanthin and ellagic acid have the potential to inhibit the UV-induced MAPK pathway in melanoma carcinogenesis as protein kinase inhibitors.

Keywords: In silico, Astaxanthin, Ellagic acid, UV radiation, MAPK pathway, melanoma carcinogenesis, skin cancer, protein kinases

1. Introduction

Skin cancers have a strong link with UV radiation from the sun. Recently, the occurrence of skin cancers due to UV induction has increased, and the risk depends on the age, gender, nature of the skin, and dosage of UV exposure. Some studies showed that exposure to the sun during childhood may also result in disease later in life. These epidemiological studies become hard to predict as the results may be biased because of the inefficient recollection of early life events by the participants of the study [1].

The prolonged exposure to UV radiation alters the signaling networks and creates a disturbance in the homeostasis of the skin, causing cell destruction, which certainly leads to skin carcinogenesis. The prevention of the initiation stage of cancer using chemoprevention agents was hard as the initiation stage is irreversible and lasts only for a short duration. However, targeting the promotion stage with chemoprevention agents is quite successful as the promotion stages are reversible and time-consuming. The promotion stage is characterized by the mutation in the tumor suppressor genes (like p53), overexpression of inflammatory

transcription factors (like AP-1, NF-κB), and fluctuations in the production of pro-inflammatory cytokines and inflammatory enzymes (like COX-2). And so, most of the studies aimed to develop chemoprevention agents targeting signaling molecules that are oncogenic [2].

The fluctuations in ROS production due to UV exposure produce EGFR ligands and pro-amphiregulin at the cell membrane. The EGFR undergoes a conformational change when bound to free amphiregulin and subsequently activates itself through dimerization. Studies confirmed the increase in amphiregulin post-UV exposure. Further, the epidermal growth factor receptors activate various signaling pathways (including p38, JNK, ERK) of skin carcinogenesis induced by UV radiation [2]. Inhibition of these pathways helps in skin cancer prevention and treatment.

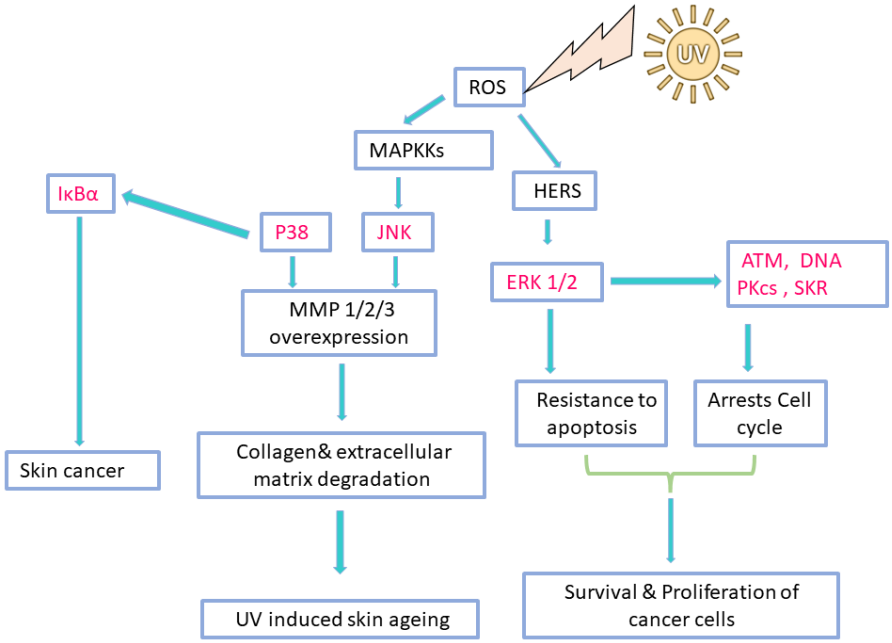

Figure 1. Flow diagram representing the role of protein kinases in UV-induced skin carcinogenesis [3–6].

Astaxanthin, a keto-carotenoid, shows antioxidant properties due to the conjugated double bond present at the center. The pharmacological approaches were used to examine Astaxanthin's affinity targets, signaling pathways, and related disease applications [7-8]. It has the ability to decrease ROS production and apoptosis induced by UV radiation, thereby being found to produce beneficial effects. It is also said to have anti-lipid peroxidation, antiproliferative, wound healing, and positive effects on skin damage due to DNA repair and antitumor effects [9].

Ellagic acid is an antioxidant said to inhibit the UVA-mediated apoptosis of human keratinocyte cells. It also suppressed ROS production and MDA formation due to UVA exposure. The antioxidant capacity of ellagic acid is linked to the overexpression of SOD and HO-1[10]. Studies also showed that upon oxidation by tyrosinase, ellagic acid can reduce the o-quinones and semi-quinones, thereby inhibiting the melanogenesis process. It also can alter the redox status of the cell [11]. Ellagic acid has the ability to bind and inhibit the activity of PDK3 kinase[12]. Ellagic acid is said to possess anticancer properties, and its mechanism was studied using several bioinformatics tools and databases [13].

Luteolin is a natural flavonoid that possesses antitumor activity because of its ability to inhibit the induction of cell cycle disruption, apoptosis, and inhibition of cell proliferation and migration[14]. Luteolin regulates signaling molecules of skin cancer (like NF-κB, JAK–STAT, TLR) and suppresses the activity of pro-inflammatory mediators[15]. It is proven that Luteolin

reduces inflammation by counteracting MAPK, NF-κB, and JAK-STAT inflammatory pathways[16].

Taxifolin, is a bioactive flavonoid and a dietary component that can be isolated from plant sources like onion, tamarind, milk thistle, and French maritime[17]. It prevented several malignancies due to its antioxidant capacity [18]. Studies showed that by inactivation of OCT4 and PI3K, Taxifolin inhibited epithelial-mesenchymal transition and stemness in lung cancer cells [19]. Taxifolin exhibits antitumor activity against UV-induced skin cancers by targeting EGFR and PI3K [20].

After finding the appropriate protein kinase targets, the efficiency of Astaxanthin and ellagic acid against UV-mediated skin cancer pathways is analyzed in this study using silico methods. Luteolin and Taxifolin are taken as standard drugs due to their proven anticancer properties.

2. Materials and Methods

2.1. Protein preparation.

We have searched for protein kinase targets of UV-mediated skin cancers to verify the anti-radical properties of Ellagic acid and Astaxanthin. Reviewing several literatures, we finalized seven protein kinase targets: JNK, p38, IκBα, DNA-PKcs, ERK ½, ATM, and SKR. After this, two proteins for each kinase target were retrieved from the protein data bank in PDB formats. The selected proteins are of human origin, and the PDB code of selected proteins are 3O2M, 4X21, 5TCO, 7MGJ, 4KIK, 5SFD, 1ZRZ, 5MRD, 1ZC0, 3VP4, 3LYM, 5G55, 1L60 and 1WBU respectively. These proteins were then prepared using UCSF Chimera 1.16, where all the ions, ligands, and chains (except interacting chains) were removed [21].

2.2 Ligand preparation

The compounds of interest, Astaxanthin, and ellagic acid, are the ligand molecules that are to be docked with the chosen proteins. Luteolin and Taxifolin are the two anti-cancerous drugs that are taken as standard ligand molecules. The 3-dimensional model of all four ligands was retrieved from the PubChem database as an SDF file. UCSF Chimera 1.16 is used to convert all these ligands from SDF format to PDB format.

Table 1. Kinase targets for UV mediated Skin cancers and PDB ID of respective proteins.

PROTEIN KINASES	PDB ID of Proteins
JNK	3O2M
	4X21
p38	5TCO
	7MGJ
IκBα	4KIK
	5SFD
DNA-PKcs	1ZRZ
	5MRD
ERK1/2	1ZC0
	3VP4
ATM	3LYM
	5G55
SKR	1L60
	1WBU

Table 2. Ligands that are docked with protein and their PubChem ID

LIGAND	PubChem ID
Astaxanthin	5281224
Ellagic Acid	5281855
Luteolin	5280445
Taxifolin	439533

2.3. Active sites of protein kinase targets.

Active sites of the proteins are where the ligands interact with the proteins. So, to perform Insilico studies, it is important to determine the active sites of the chosen protein. In this study, the active sites are found using the website version of CASTp 3.0 [22], and in some instances, bounded ligand positions are spotted in PMV-1.5.6 software; in those positions, the ligand of interest is bound.

Table 3. Active sites of protein and Grid size & Grid center coordinates.

Protein Kinase Targets	PDB ID of Proteins	Active Sites	Grid size (x ,y ,z)	Grid center (x, y, z) coordinates
JNK	3O2M	LYS55,ASP151	40,24,40	30.111,87.50,44.444
	4X21	ASN93,VAL189	40,36,40	30.24,36.796,59.85
P38	5TCO	LYS53,GLU71,MET109,SER154,ASP168,TRP197,LEU262	40,40,40	19.328,8.443,-26.496
	7MGJ	ILE69,ALA88,LYS90,GLU109,VAL121,ILE122,GLN140, TYR141,ILE142,LEU177,HIS186,VAL204,ALA205,ASP206, PHE207	34,36,40	5.666,-6.835,0.668
IκBα	4KIK	ARG26,GLY44,PRO98,LEU99,LEU152,ARG165,LEU166	24,28,24	-11.545,18.899,22.764
	5SFD	VAL678,ILE692,TYR693,PHE696,PRO712, GLU721,GLN726, TYR729	28,26,28	-10.11,37.615,-7.985
DNA-PKcs	1ZRZ	ILE251,VAL259,LYS274,GLU324,VAL326, ASP330,ASP373, LEU376,THR386	26,30,28	48.56,27.73,-54.9
	5MRD	VAL94,SER111,GLY126,GLU160,ILE162,GLU166,ILE223	26,28,28	93.95,-13.22,8.9
ERK 1/2	1ZC0	ASP236,CYS270,GLN314	40,40,40	45.271,39.74,9.938
	3VP4	SER286,ASN335,GLU381,ASN388,TYR414, TYR466,VAL484	40,40,40	17.076,-6.629,-12.755
ATM	3LYM	GLU35,ASP52,ASP101	40,40,40	3.649,21.009,21.9
	5G55	GLY829,ILE830,ILE831,PHE832,LYS833,HIS834,GLY835,ASP836,ASP837,LEU838,LEU864,865LEU,PRO866,TYR867,GLY868,CYS869,ILE870,SER871,THR872,PHE961,HIS962,ILE963,ASP964,PHE965,GLY966,HIS967,ILE968,LEU969	40,40,40	22.457,28.255,-9.624
SKR	1L60	ASP10,GLU11,ILE17,ASP20,LEU32,ALA41, ASN132	40,40,40	35.146,16.448,5.942
	1WBU	LYS7,ARG10,HIS12,LY66,ARG85,HIS119	40,40,40	31.421,0.19,13.744

2.4. Docking preparation.

The pre-processed proteins obtained from UCSF Chimera 1.16 were further processed using PMV-1.5.6 software, where the water molecules were removed, and additional charges were added to the proteins. These proteins were then used for Insilico docking.

2.5 Molecular docking process.

The docking was performed using AutoDock Vina and PMV-1.5.6 software. The prepared proteins were docked against all four ligands (Ellagic acid, Astaxanthin, Luteolin, and Taxifolin). Active sites were used to generate grid boxes. PDBQT files of proteins and ligands are generated. PDBQT files and the grid box values were noted in the configuration file. The

output log file which is generated during the Vina run, contains affinity values and RMSD (Root Mean Square Deviation) values. In most cases, the output ligand 1 will have the highest affinity scores than the rest of the output ligands generated [24-25].

2.6 Protein–Ligand interaction visualization.

The 2D and 3D interactions of protein and ligand are analyzed using BIOVIA Discovery Studio Visualizer-2021 software [25]**,** where the number of hydrogen bonds between protein and ligand is visualized in both 2-Dimension and 3-Dimension. The distances of the H – Bonds are also noted. The Pymol software is used to visualize the active sites and protein-ligand interactions. PMV-1.5.6 software is used to visualize the affinity of a protein for the ligands.

3. Results and Discussion

Following the above-mentioned procedures, docking is performed for two proteins of each protein kinase target in UV mediated skin carcinogenesis pathway with Astaxanthin, ellagic acid as a compound of interest, and standard drugs such as Luteolin and Taxifolin.

3.1 Active sites and protein-ligand interactions.

Figures 2-8 depict the interactions between the 14 chosen proteins of 7 different kinases and the ligands astaxanthin, ellagic acid, Luteolin, and Taxifolin. In the images generated using Pymol software, the proteins are oriented in such a way that their active sites and interacting ligands are visible. The highlighted parts of the proteins are the active sites where the ligands will get attached to the protein. In order to show variations in the images for better visualization, each ligand is assigned a color code as per the colors available in the Pymol software, which is represented in Table 4.

Table 4. Color of ligands interacting with proteins in the 3D visualization generated using Pymol software.

LIGAND	COLOR (as per Pymol software)
Astaxanthin	Deep salmon
Ellagic acid	Green cyan
Luteolin	Yellow
Taxifolin	Hot pink

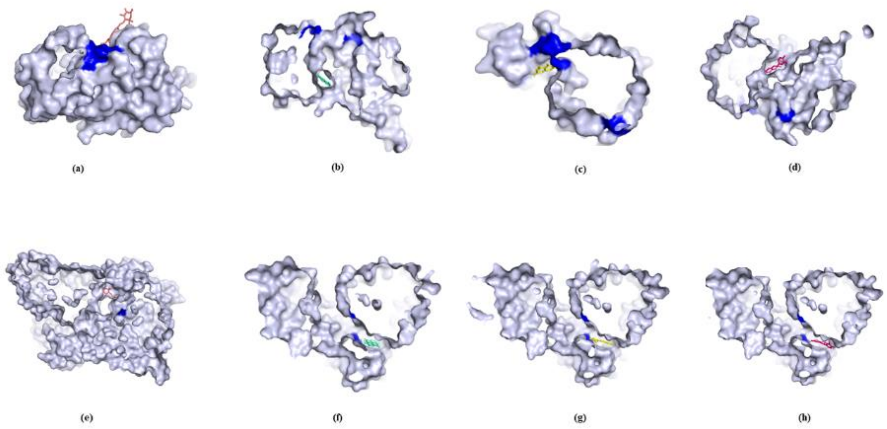

Figure 2. Representation of active sites and Interactions of JNK proteins (i) 3O2M with **(a)** Astaxanthin, **(b)** Ellagic acid, **(c)** Luteolin, **(d)** Taxifolin, and (ii) 4X21 with **(e)** Astaxanthin, **(f)** Ellagic acid, **(g)** Luteolin, **(h)** Taxifolin.

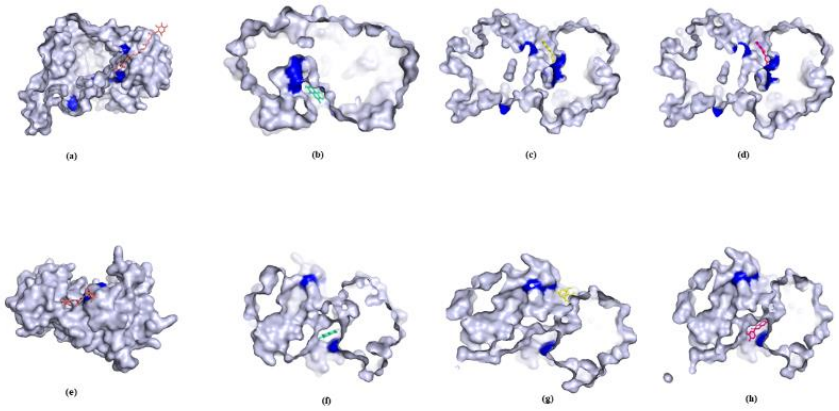

Figure 3. Representation of active sites and Interactions of p38 proteins (i) 5TCO with **(a)** Astaxanthin, **(b)** Ellagic acid, **(c)** Luteolin, **(d)** Taxifolin, and (ii) 7MGJ with **(e)** Astaxanthin, **(f)** Ellagic acid, **(g)** Luteolin, **(h)** Taxifolin.

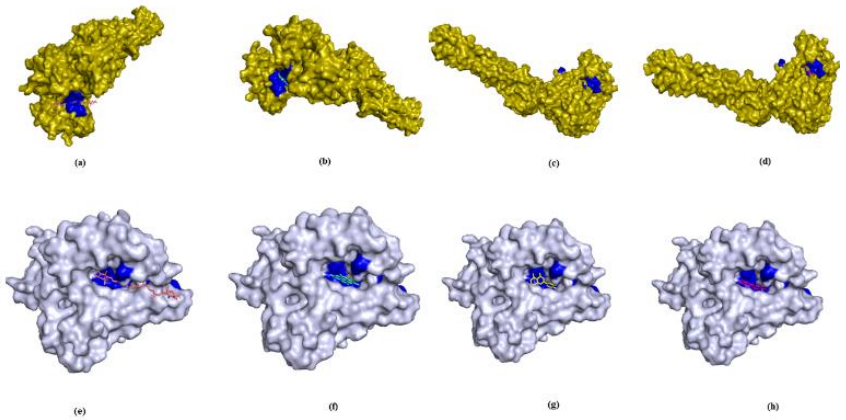

Figure 4. Representation of Active sites and Interactions of IκBα proteins (i) 4KIK with **(a)** Astaxanthin, **(b)** Ellagic acid, **(c)** Luteolin, **(d)** Taxifolin and (ii) 5SFD with **(e)** Astaxanthin, **(f)** Ellagic acid, **(g)** Luteolin, **(h)** Taxifolin.

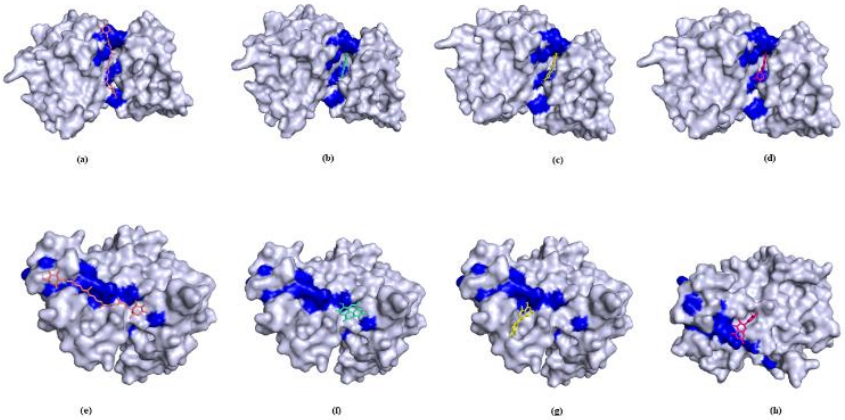

Figure 5. Representation of Active sites and Interactions of DNA-PKcs proteins (i) 1ZRZ with **(a)** Astaxanthin, **(b)** Ellagic acid, **(c)** Luteolin, **(d)** Taxifolin and (ii) 5MRD with **(e)** Astaxanthin, **(f)** Ellagic acid, **(g)** Luteolin, **(h)** Taxifolin.

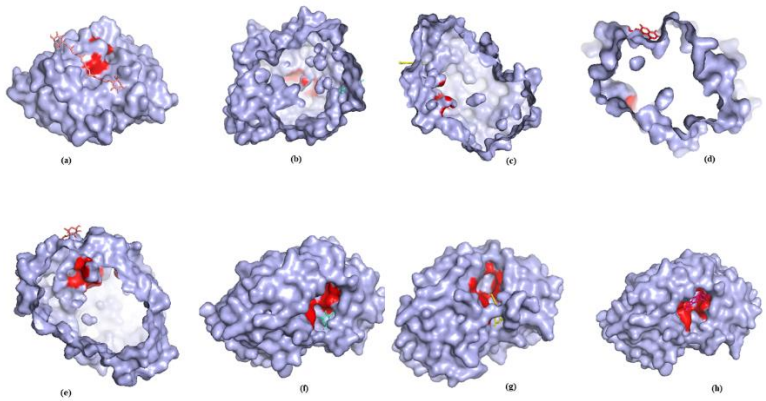

Figure 6. Representation of Active sites and Interactions of ERK 1/2 proteins (i) 1ZC0 with **(a)** Astaxanthin, **(b)** Ellagic acid, **(c)** Luteolin, **(d)** Taxifolin and (ii) 3VP4 with **(e)** Astaxanthin, **(f)** Ellagic acid, **(g)** Luteolin, **(h)** Taxifolin.

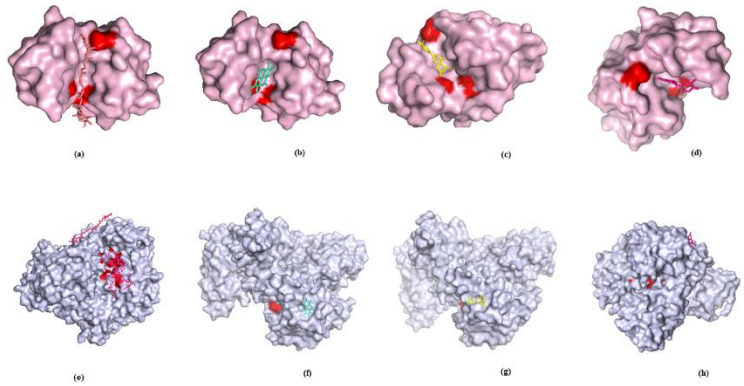

Figure 7. Representation of Active sites and Interactions of ATM proteins (i) 3LYM with **(a)** Astaxanthin, **(b)** Ellagic acid, **(c)** Luteolin, **(d)** Taxifolin, and (ii) 5G55 with **(e)** Astaxanthin, **(f)** Ellagic acid, **(g)** Luteolin, **(h)** Taxifolin.

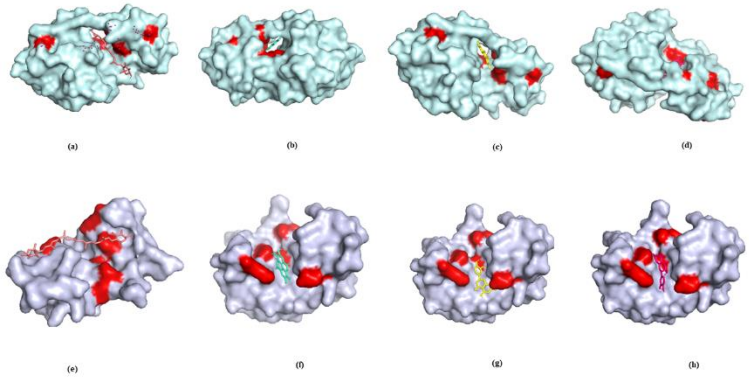

Figure 8. Representation of Active sites and Interactions of SKR proteins (i) 1L60 with **(a)** Astaxanthin, **(b)** Ellagic acid, **(c)** Luteolin, **(d)** Taxifolin, and (ii) 1WBU with **(e)** Astaxanthin, **(f)** Ellagic acid, **(g)** Luteolin, **(h)** Taxifolin.

3.2. Visualization of protein-ligand interactions.

The interactions between protein and ligand can be visualized using BIOVIA Discovery Studio. The 3D representation of protein-ligand interactions highlights the H-bond donors and acceptors and bond distances of different types of bonds between the ligand and the protein, while the 2D representation of protein-ligand interaction gives a clear picture of protein residues that take part in binding with the ligand. The 3D and 2D representations for 14 proteins with Astaxanthin, ellagic acid, Luteolin, and Taxifolin are shown in Figures 10-37.

The number of H-bonds formed between the protein and ligand, residues involved in H-bonds, and their distances are shown in Tables 5-8. The H-bonds for proteins docked with Astaxanthin, ellagic acid, Luteolin, and Taxifolin are compared in Figure 9.

Table 5. Data related to H-bonds as the result of docking between proteins and Astaxanthin.

Protein Kinases	PDB ID of Protein	Hydrogen bonds	Residues linked to H bond	Distance	Minimum Distance
JNK	3O2M	1	GLN317	2.63	2.63
	7MGJ	2	GLU509, ASP606	1.78,2.16	1.78
IκBα	4KIK	1	ARG57	2.54	2.54
	5SFD	1	THR633	2.55	2.55
DNA-PKcs	1ZRZ	1	PRO532	3.71	3.71
	5MRD	1	GLU80	3.01	3.01
ATM	3LYM	2	ARG73,ARG114	2.00,2.48	2.00
	5G55	1	ARG1052	3.08	3.08
	1WBU	5	ASN67, GLN69, GLY88, LYS91, GLU111	1.96, 2.24, 2.34, 2.50, 2.64	1.96

Table 6. Data related to H-bonds as the result of docking between proteins and ellagic acid.

Protein Kinases	Protein	Hydrogen bonds	Residues linked to H bond	Distance	Minimum Distance
JNK	3O2M	3	LYS55,ASP169	2.34,2.44,2.44	2.34
	4X21	1	SER72	2.23	2.23
	7MGJ	1	ILE585	2.23	2.23
IKBA	4KIK	1	CYS99	2.22	2.22
	5SFD	4	TYR524,ASP674,SER677	2.23,2.99,2.54,2.15	2.15
DNA-PKCS	1ZRZ	3	GLU324,VAL326	2.33,2.64,2.34	2.33
	5MRD	2	ARG129,ARG136	2.87,2.11	2.11
ERK 1/2	1ZC0	2	GLN289,ASP297	1.91,2.17	1.91
	3VP4	5	SER314, PHE322, HIS330, ALA336, ARG387	2.09, 2.12, 2.12, 2.38, 2.70	2.09
ATM	3LYM	1	TRP62	2.48	2.48
	5G55	4	LYS1000,THR1002,GLN1007,GLU1073	1.97,2.06,2.59,3.04	1.97
SKR	1L60	3	GLU22,LEU32,GLN105	1.98,2.08,2.94	1.98
	1WBU	3	HIS12,THR45,LYS66	2.01,2.18,2.33	2.01

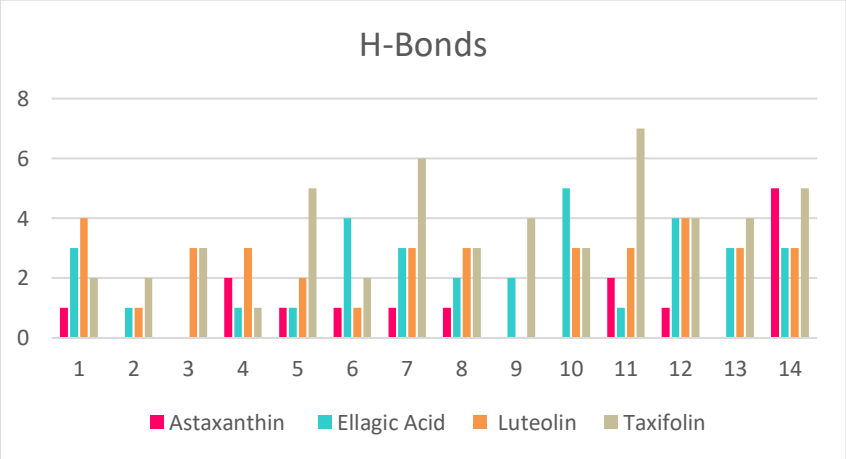

Figure 9. Bar graph representing the H-bonds of proteins with Astaxanthin, Ellagic acid, Luteolin, and Taxifolin.

Table 7. Data related to H-bonds as the result of docking between proteins and Luteolin.

Protein Kinases	Protein	Hydrogen bonds	Residues linked to H bond	Distance	Minimum Distance
JNK	3O2M	4	GLY33,GLY38,GLU109,MET111	2.00,2.27,2.27,2.80	2.00
	4X21	1	MET149	3.29	3.29
P38	5TCO	3	MET109,ALA111	1.81,1.96,2.59	1.81
	7MGJ	3	GLN540,SER549	2.28,2.60,2.74	2.28
IκBα	4KIK	2	GLU61,ASP166	2.9,1.33	2.9
	5SFD	1	GLN726	2.4	2.4
	1ZRZ	3	TYR256,VAL326,ASP387	2.2,2.11,1.94	2.2

Protein Kinases	Protein	Hydrogen bonds	Residues linked to H bond	Distance	Minimum Distance
DNA-PKcs	5MRD	3	ASN119,GLN150	1.81,2.69,1.98	1.81
	3VP4	3	SER314,MET333	2.13,2.56,2.80	2.13
ATM	3LYM	3	GLN57,ASN59,ASP101	2.17,2.75,3.05	2.17
	5G55	4	LYS1001,GLN1010,LYS1066	1.81,2.34,2.74,2.75	1.81
SKR	1L60	3	GLU20,GLY30,ARG137	1.88,2.57,2.74	1.88
	1WBU	3	HIS12,ASN44,SER123	1.83,1.99,3.05	1.83

Table 8. Data related to H-bonds as the result of docking between proteins and Taxifolin.

Protein Kinases	Protein	Hydrogen bonds	Residues linked to H bond	Distance	Minimum Distance
JNK	3O2M	2	GLY38, MET111	2.15, 2.68	2.15
	4X21	2	MET146, MET149	2.18, 2.93	2.18
P38	5TCO	3	THR106, MET109, ALA111	1.82, 1.97, 2.58	1.82
IκBα	4KIK	5	LYS44, GLU61	2.34, 2.26, 2.54, 2.53, 2.46	2.34
	5SFD	2	THR633, ASP674	2.84, 2.42	2.84
DNA-PKcs	1ZRZ	6	TYR256, GLU324, VAL326, ASN374, ASP38	2.03, 2, 2.71, 2.91, 2.2, 2.56	2.03
	5MRD	3	LEU137, LEU145, TYR146	2.34, 3.03, 2.26	2.34
ERK 1/2	1ZC0	4	LYS1001, GLN1010, LYS1066, ARG1076	1.97, 2.14, 2.57, 2.58	1.97
	3VP4	3	SER314, MET333	2.17, 2.80, 2.84	2.17
ATM	3LYM	7	ASP48.LEU56, GLN57, ASN59, TRP63	1.78, 2.03, 2.14, 2.41, 2.63, 2.93, 3.08	1.78
	5G55	4	GLN1010, ARG1076	1.97, 2.40, 2.58, 2.61	1.97
SKR	1L60	4	GLU11, TYR18, GLU22, GLN105	1.90, 2.28, 2.29, 2.41	1.90
	1WBU	5	HIS12, LYS41, THR45, SER123	1.78, 1.88, 2.08, 2.56, 2.64	1.78

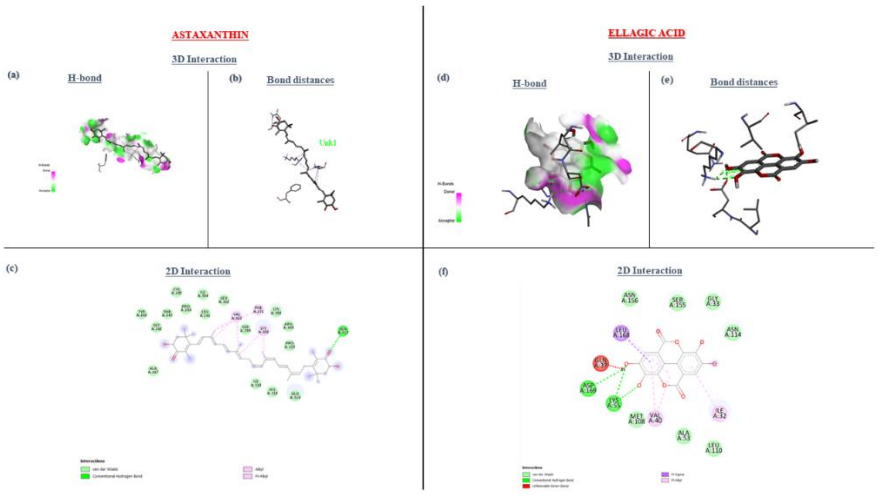

Figure 10. 2D and 3D representation of 3O2M-Astaxanthin and 3O2M-Ellagic acid interactions.

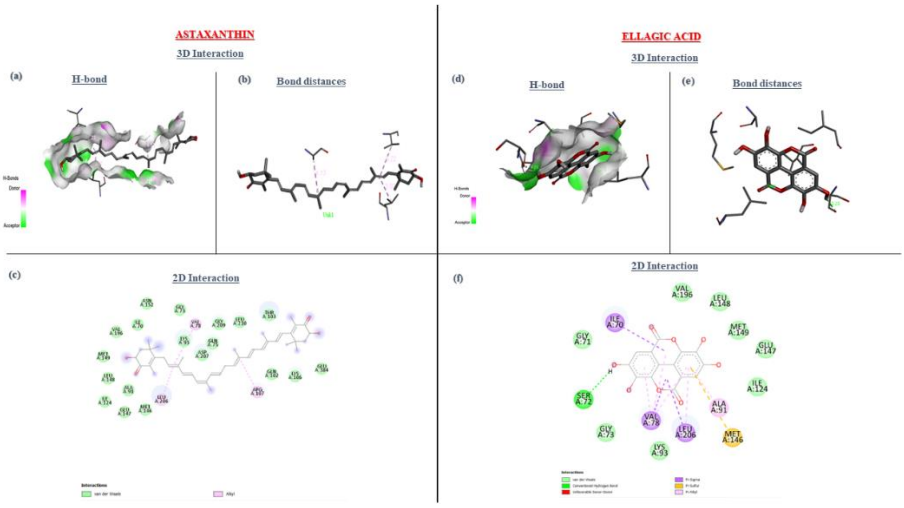

Figure 11. 2D and 3D representation of 4X21-Astaxanthin and 4X21-Ellagic acid interactions.

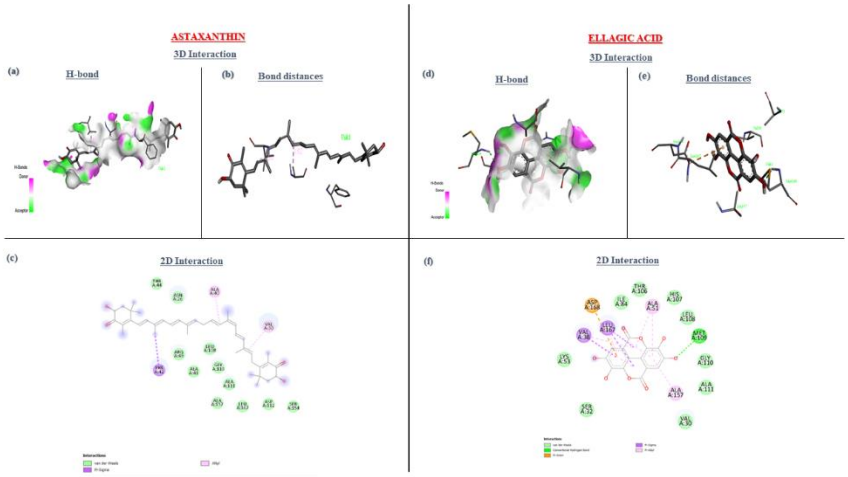

Figure 12. 2D and 3D representation of 5TCO-Astaxanthin and 5TCO-Ellagic acid interactions.

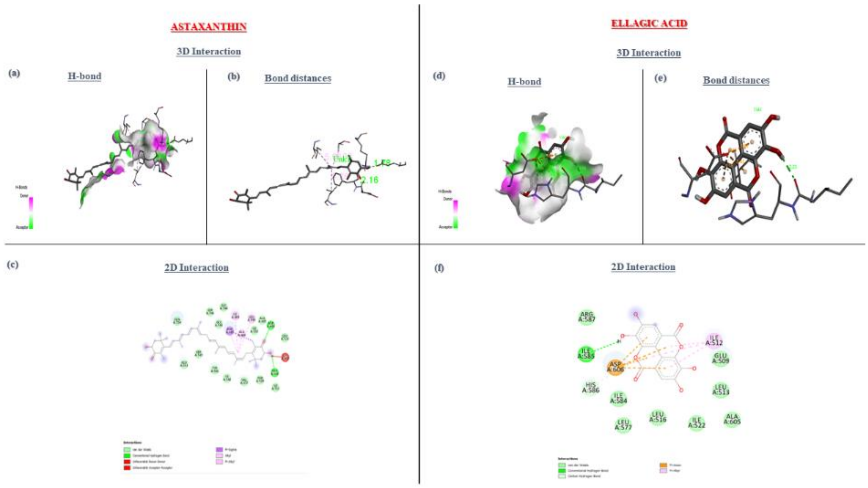

Figure 13. 2D and 3D representation of 7MGJ-Astaxanthin and 7MGJ-Ellagic acid interactions.

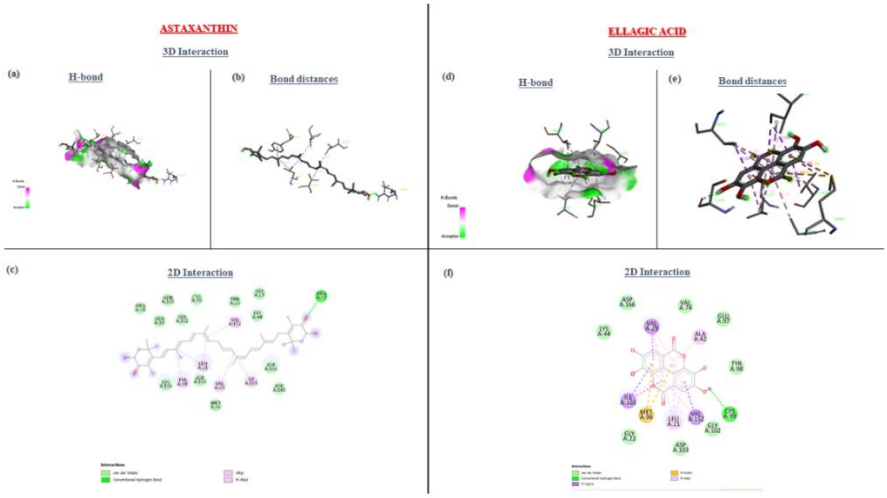

Figure 14. 2D and 3D representation of 4KIK-Astaxanthin and 4KIK-Ellagic acid interactions.

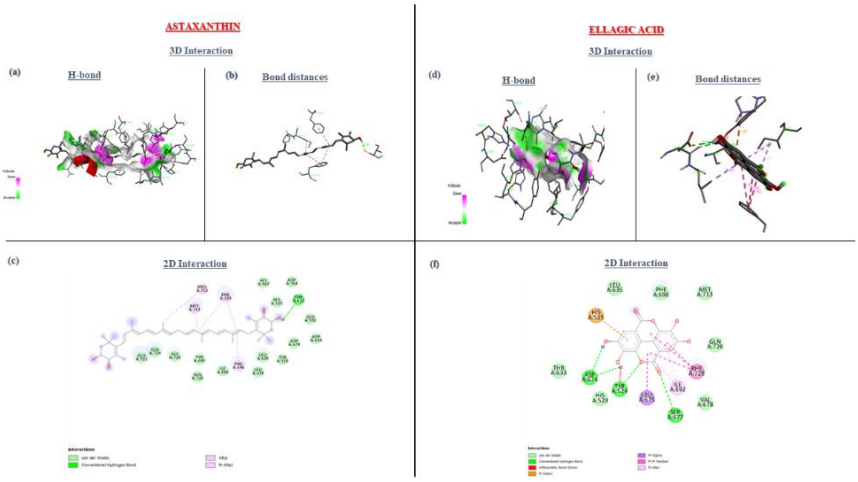

Figure 15. 2D and 3D representation of 5SFD-Astaxanthin and 5SFD-Ellagic acid interactions.

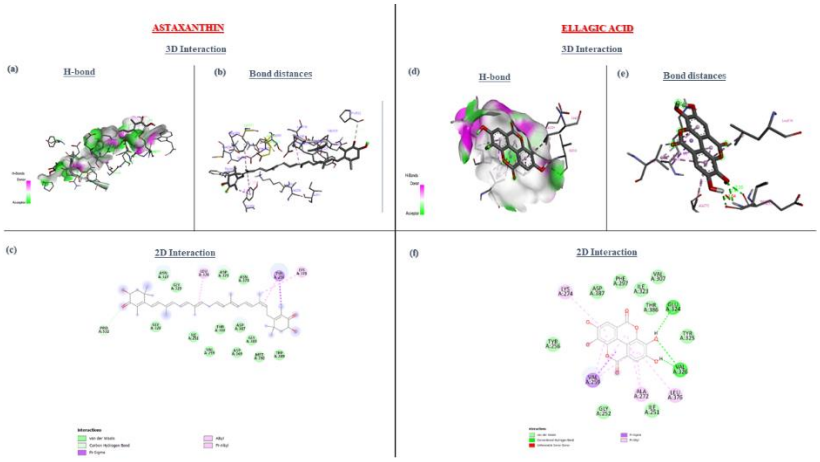

Figure 16. 2D and 3D representation of 1ZRZ-Astaxanthin and 1ZRZ-Ellagic acid interactions.

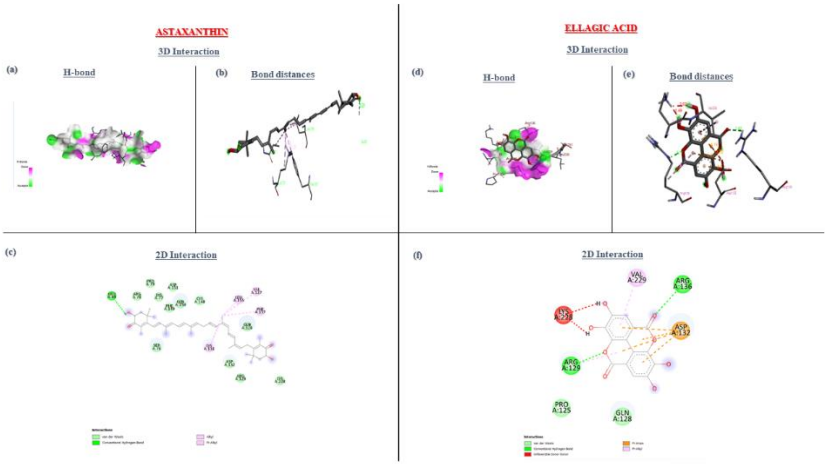

Figure 17. 2D and 3D representation of 5MRD-Astaxanthin and 5MRD-Ellagic acid interactions.

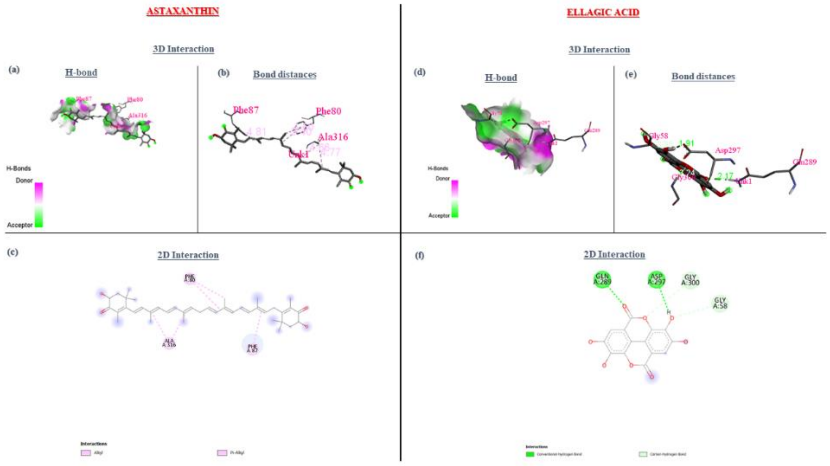

Figure 18. 2D and 3D representation of 1ZC0-Astaxanthin and 1ZC0-Ellagic acid interactions.

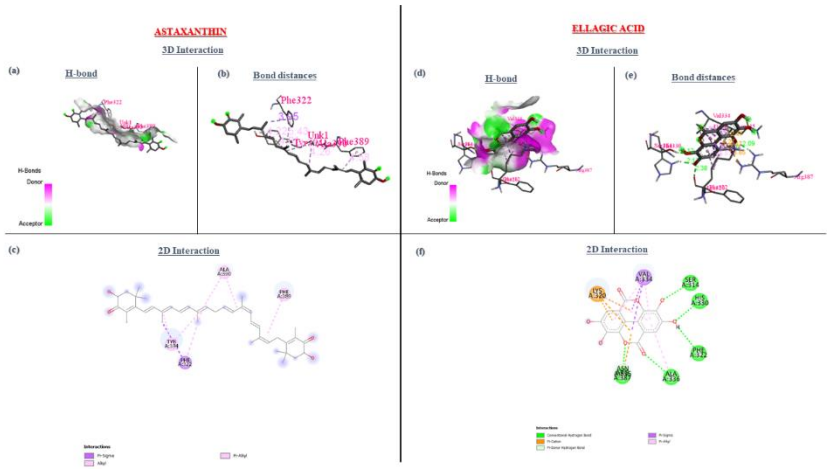

Figure 19. 2D and 3D representation of 3VP4-Astaxanthin and 3VP4-Ellagic acid interactions.

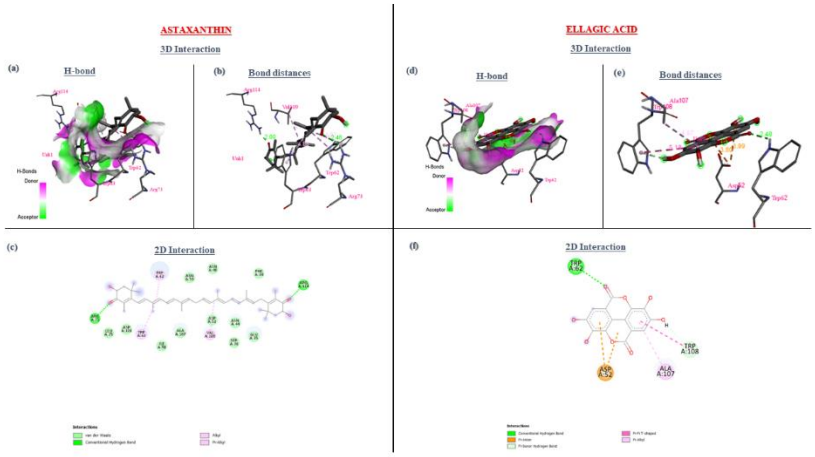

Figure 20. 2D and 3D representation of 3LYM-Astaxanthin and 3LYM-Ellagic acid interactions.

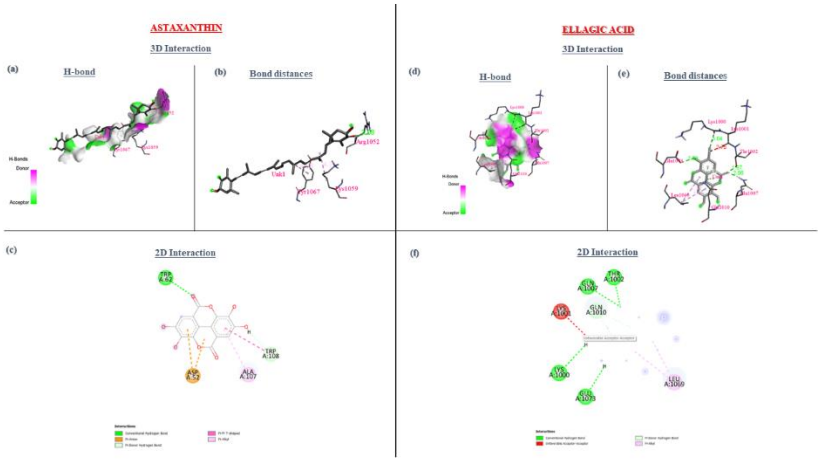

Figure 21. 2D and 3D representation of 5G55-Astaxanthin and 5G55-Ellagic acid interactions.

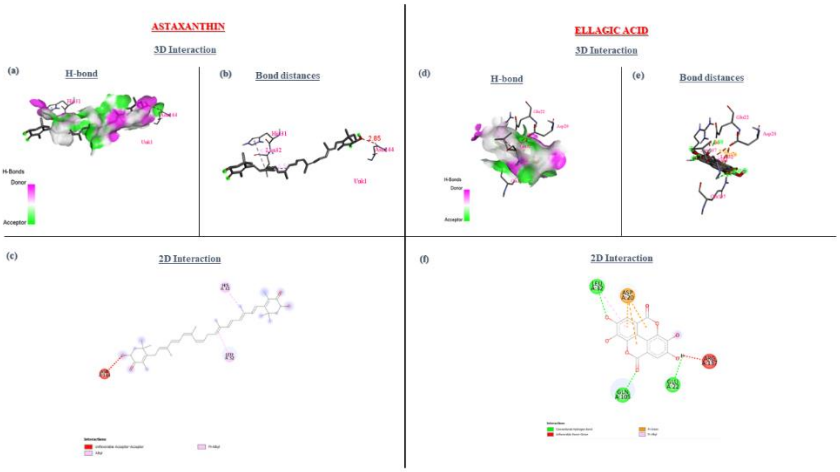

Figure 22. 2D and 3D representation of 1L60-Astaxanthin and 1L60-Ellagic acid interactions.

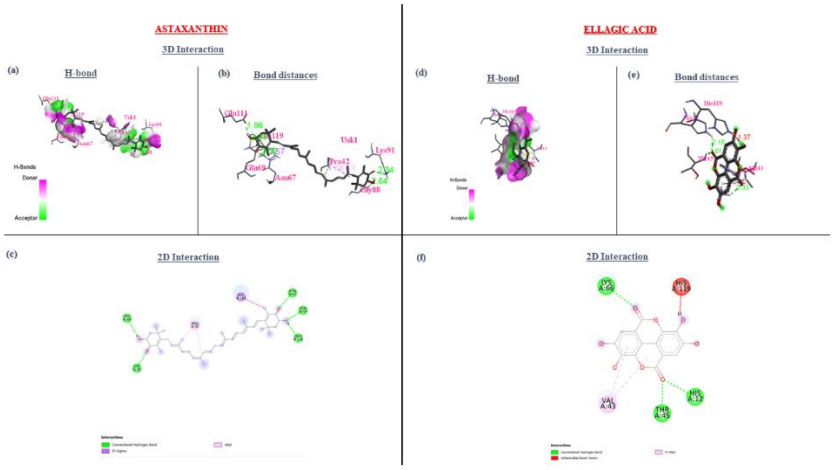

Figure 23. 2D and 3D representation of 1WBU-Astaxanthin and 1WBU-Ellagic acid interactions.

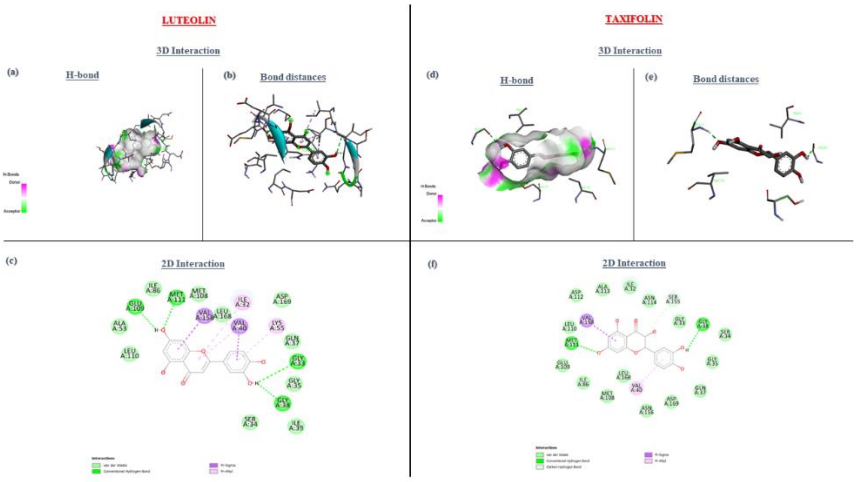

Figure 24. 2D and 3D representation of 3O2M-Luteolin and 3O2M-Taxifolin interactions.

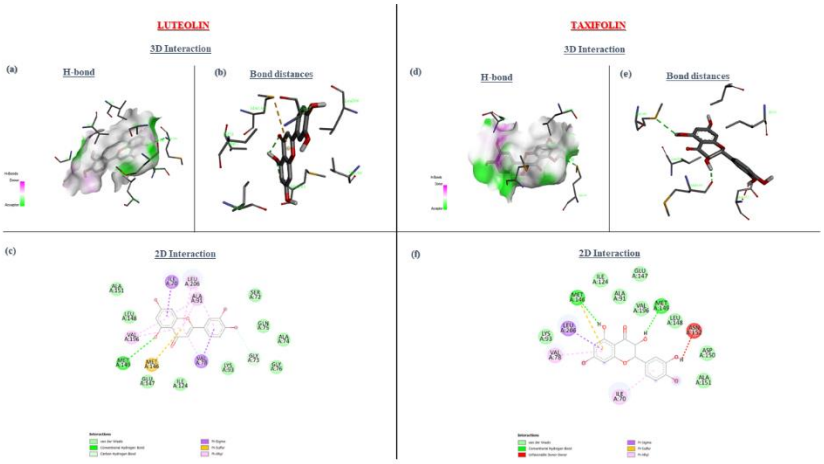

Figure 25. 2D and 3D representation of 4X21-Luteolin and 4X21-Taxifolin interactions.

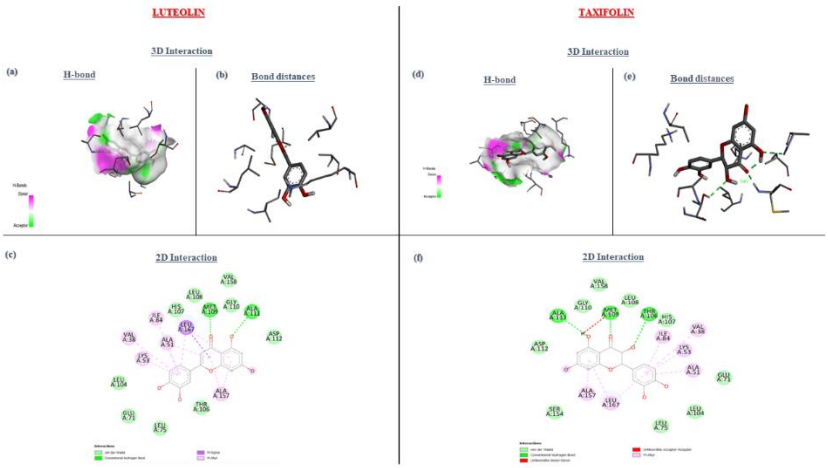

Figure 26. 2D and 3D representation of 5TCO-Luteolin and 5TCO-Taxifolin interactions.

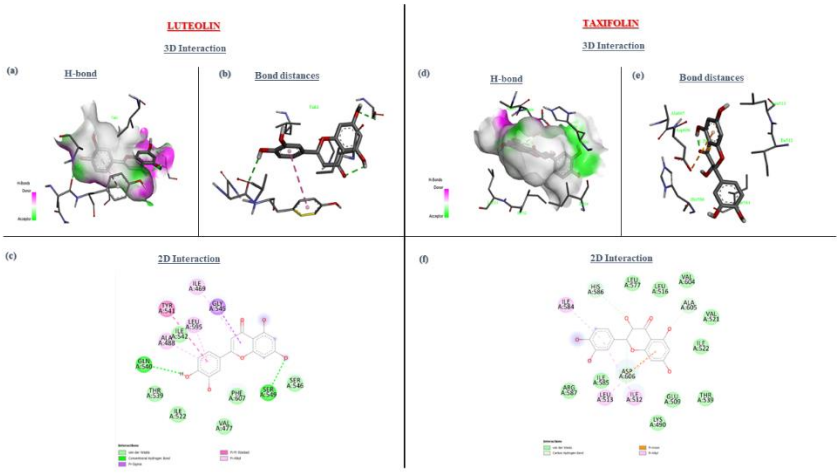

Figure 27. 2D and 3D representation of 7MGJ-Luteolin and 7MGJ-Taxifolin interactions.

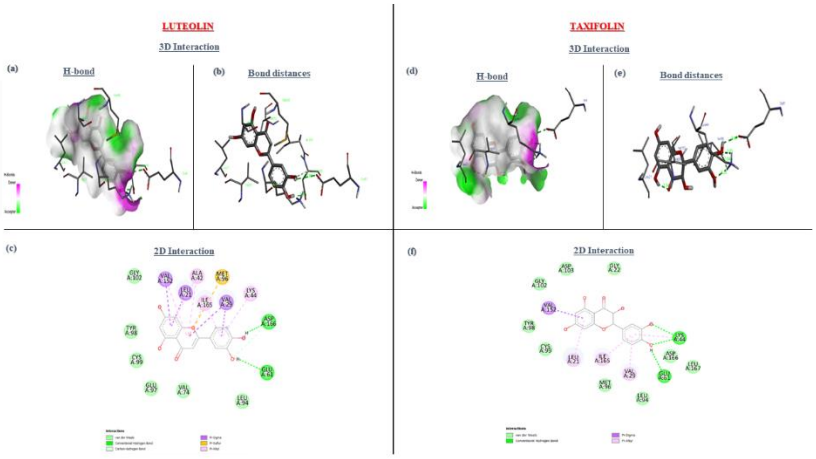

Figure 28. 2D and 3D representation of 4KIK-Luteolin and 4KIK-Taxifolin interactions.

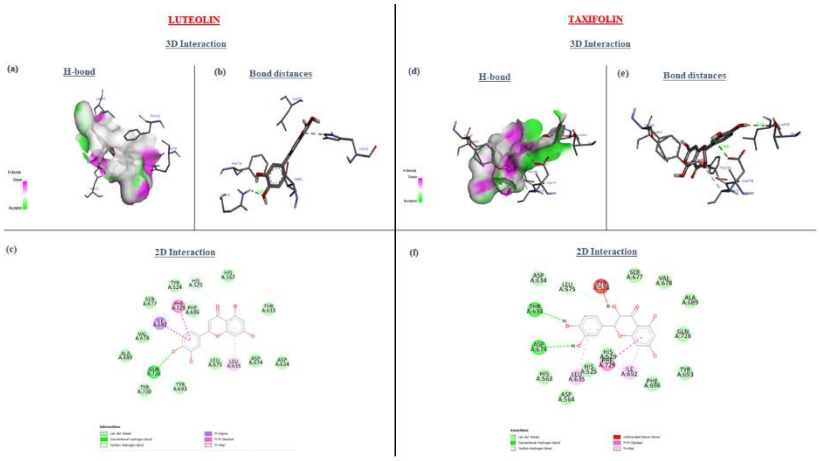

Figure 29. 2D and 3D representation of 5SFD-Luteolin and 5SFD-Taxifolin interactions.

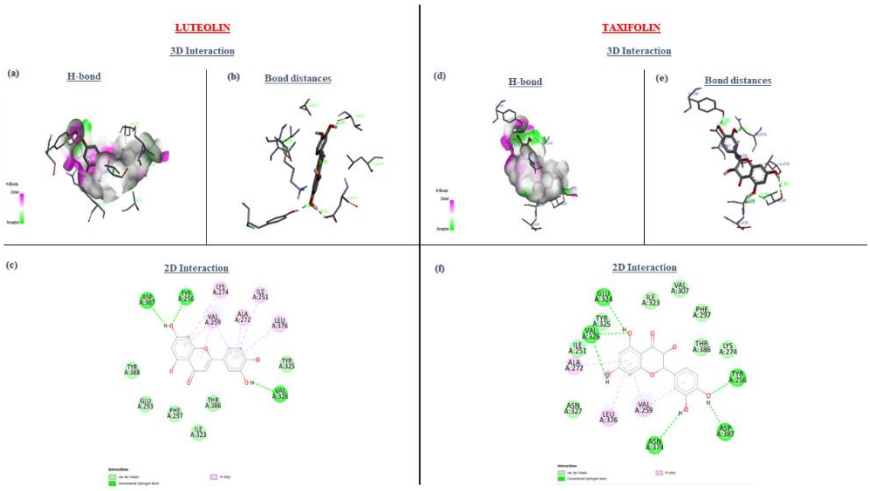

Figure 30. 2D and 3D representation of 1ZRZ-Luteolin and 1ZRZ-Taxifolin interactions.

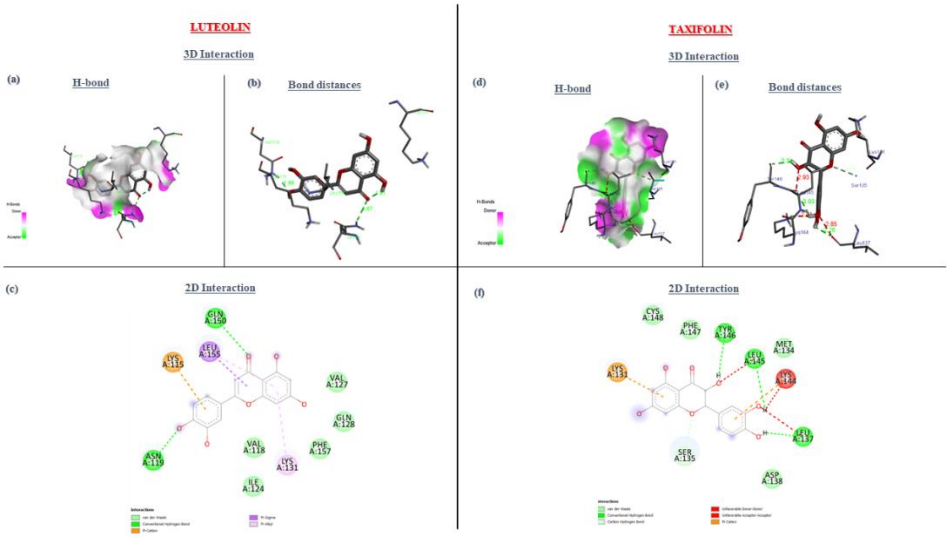

Figure 31. 2D and 3D representation of 5MRD-Luteolin and 5MRD-Taxifolin interactions.

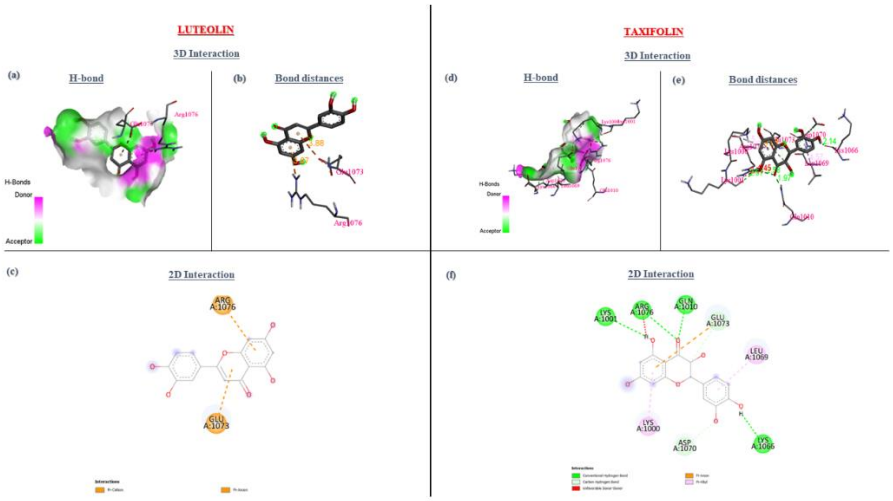

Figure 32. 2D and 3D representation of 1ZC0-Luteolin and 1ZC0-Taxifolin interactions.

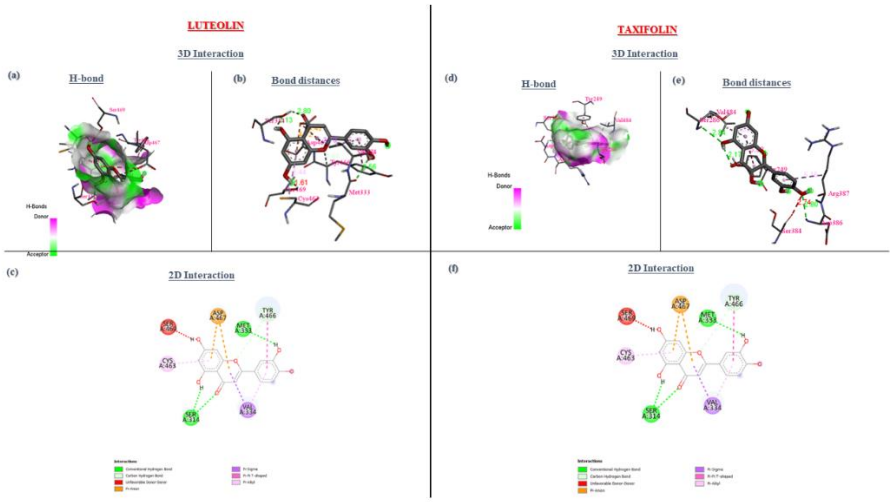

Figure 33. 2D and 3D representation of 3VP4-Luteolin and 3VP4-Taxifolin interactions.

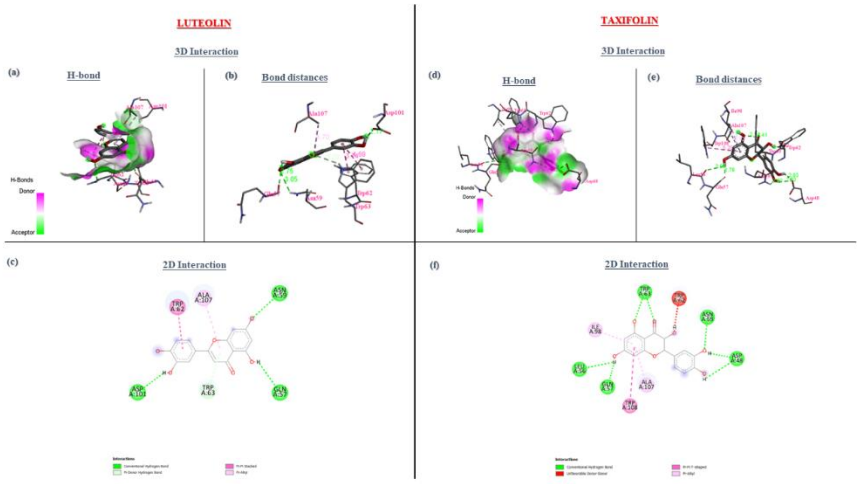

Figure 34. 2D and 3D representation of 3LYM-Luteolin and 3LYM-Taxifolin interactions.

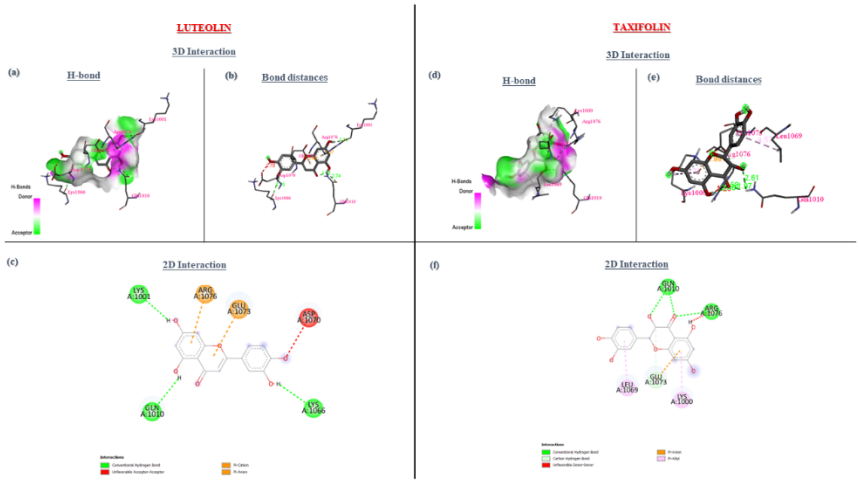

Figure 35. 2D and 3D representation of 5G55-Luteolin and 5G55-Taxifolin interactions.

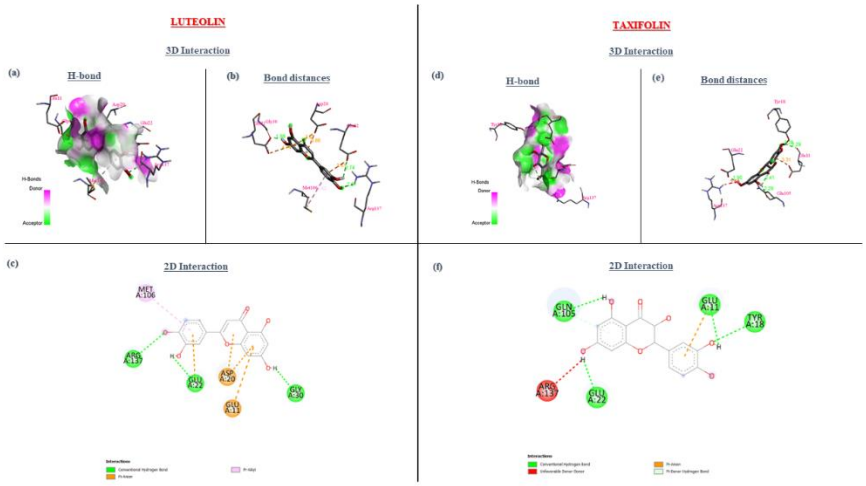

Figure 36. 2D and 3D representation of 1L60-Luteolin and 1L60-Taxifolin interactions.

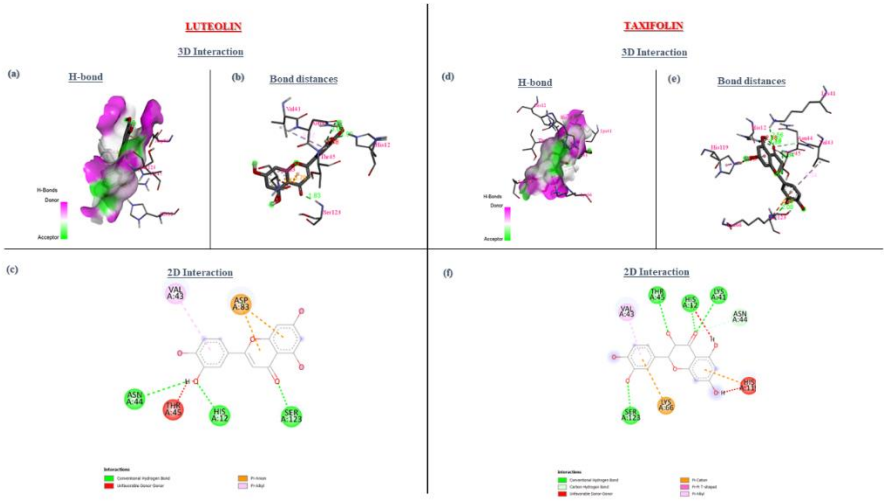

Figure 37. 2D and 3D representation of 1WBU-Luteolin and 1WBU-Taxifolin interactions.

3.3. Affinity scores and RMSD values.

The affinity scores are found in the log files generated as output in the AutoDock Vina software. For the best docking results, the affinity scores should be high and RMSD values less than 2 Å. Among the output files generated, the **output ligand 1** will have better affinity scores and low RMSD values in most cases. Further, the affinity between the protein and ligands can be visualized using PMV 1.5.6 software (Figures 38-44).

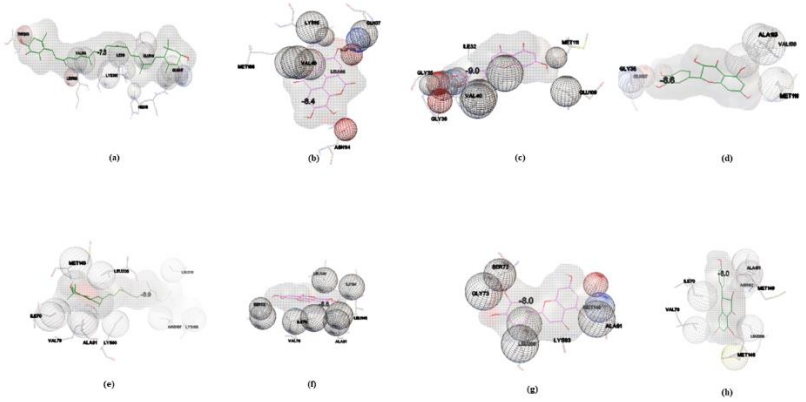

Figure 38. Affinity of JNK proteins: (i) 3O2M for **(a)** Astaxanthin, **(b)** Ellagic acid, **(c)** Luteolin, **(d)** Taxifolin, and (ii) 4X21 for **(e)** Astaxanthin, **(f)** Ellagic acid, **(g)** Luteolin, **(h)** Taxifolin.

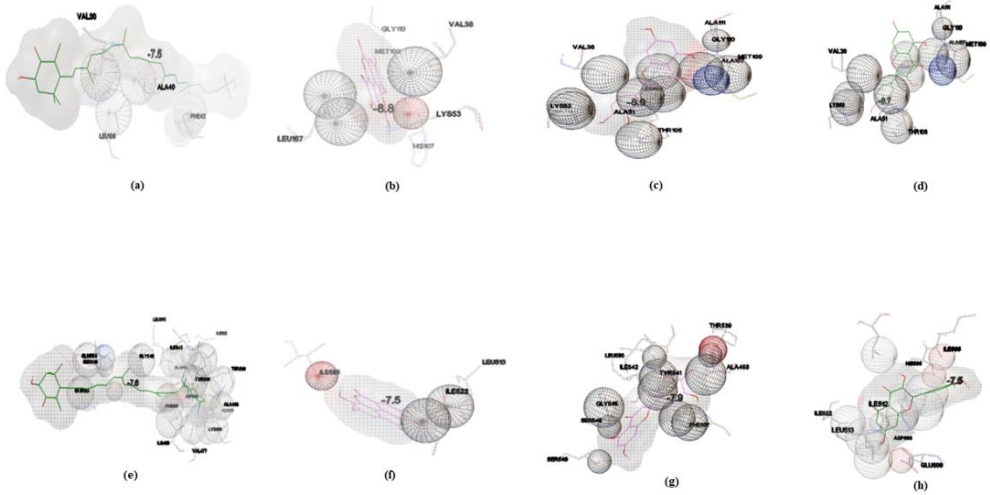

Figure 39. Affinity of p38 proteins: (i)5TCO for **(a)** Astaxanthin, **(b)** Ellagic acid, **(c)** Luteolin, **(d)** Taxifolin, and (ii) 7MGJ for **(e)** Astaxanthin, **(f)** Ellagic acid, **(g)** Luteolin, **(h)** Taxifolin.

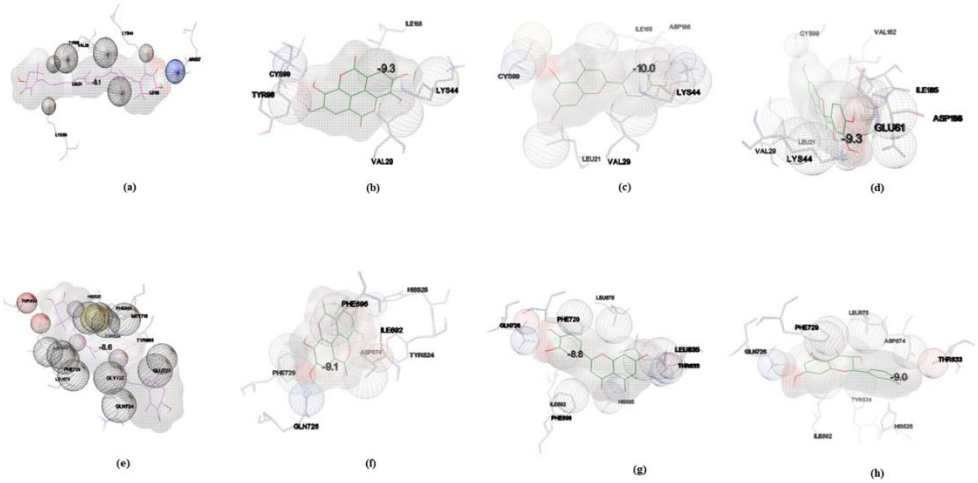

Figure 40. Affinity of IκBα proteins: (i) 4KIK for **(a)** Astaxanthin, **(b)** Ellagic acid, **(c)** Luteolin, **(d)** Taxifolin, and (ii) 5SFD for **(e)** Astaxanthin, **(f)** Ellagic acid, **(g)** Luteolin, **(h)** Taxifolin.

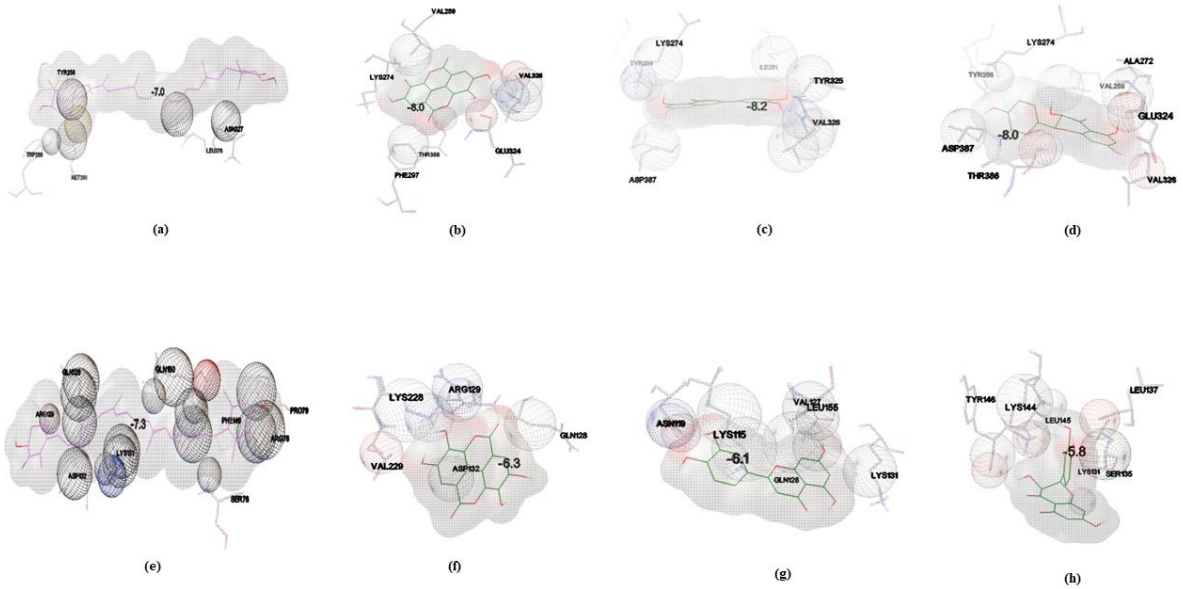

Figure 41. Affinity of DNA-PKcs proteins: (i) 1ZRZ for **(a)** Astaxanthin, **(b)** Ellagic acid, **(c)** Luteolin, **(d)** Taxifolin, and (ii) 5MRD for **(e)** Astaxanthin, **(f)** Ellagic acid, **(g)** Luteolin, **(h)** Taxifolin.

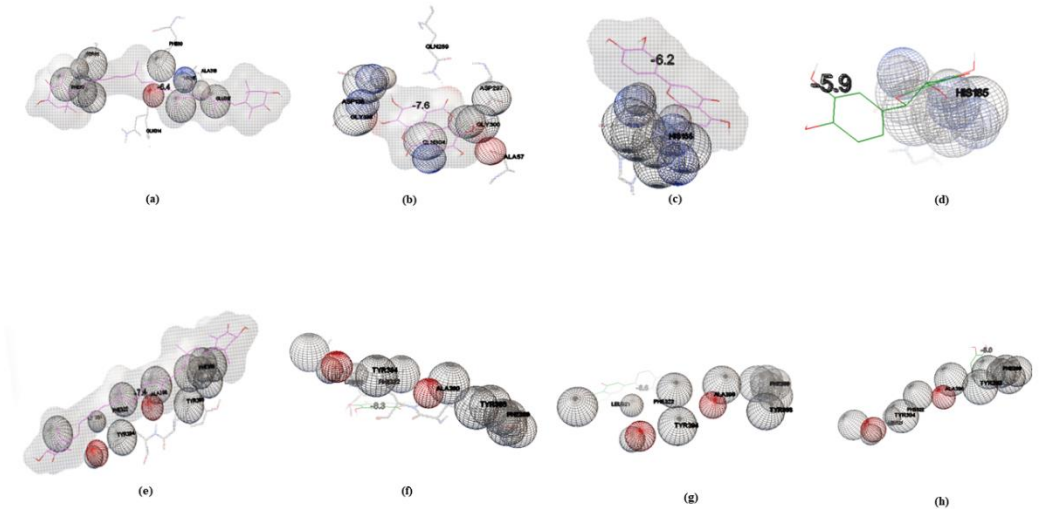

Figure 42. Affinity of ERK1/2 proteins: (i) 1ZC0 for **(a)** Astaxanthin, **(b)** Ellagic acid, **(c)** Luteolin, **(d)** Taxifolin, and (ii) 3VPM for **(e)** Astaxanthin, **(f)** Ellagic acid, **(g)** Luteolin, **(h)** Taxifolin.

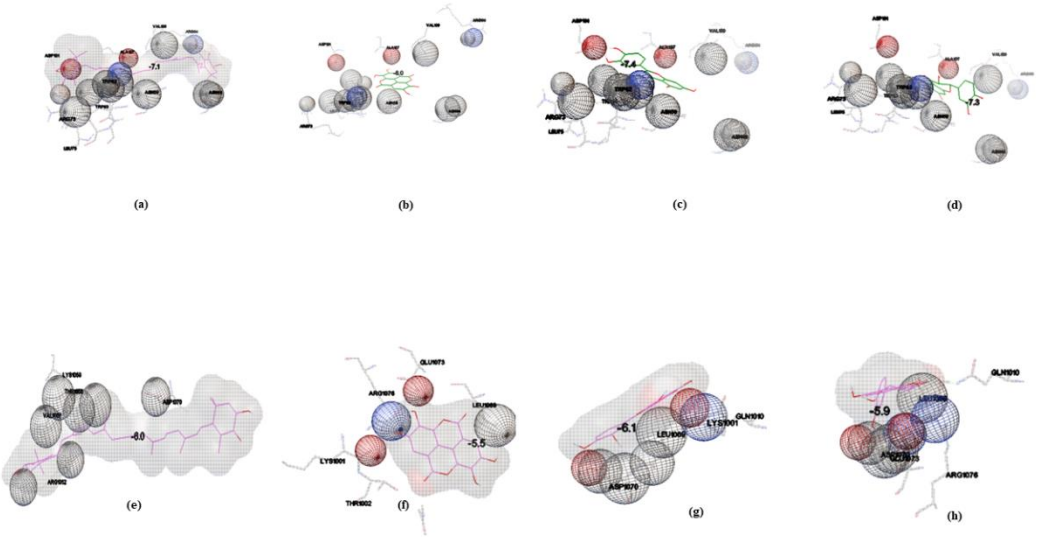

Figure 43. Affinity of ATM proteins: (i) 3LYM for **(a)** Astaxanthin, **(b)** Ellagic acid, **(c)** Luteolin, **(d)** Taxifolin, and (ii) 5G55 for **(e)** Astaxanthin, **(f)** Ellagic acid, **(g)** Luteolin, **(h)** Taxifolin.

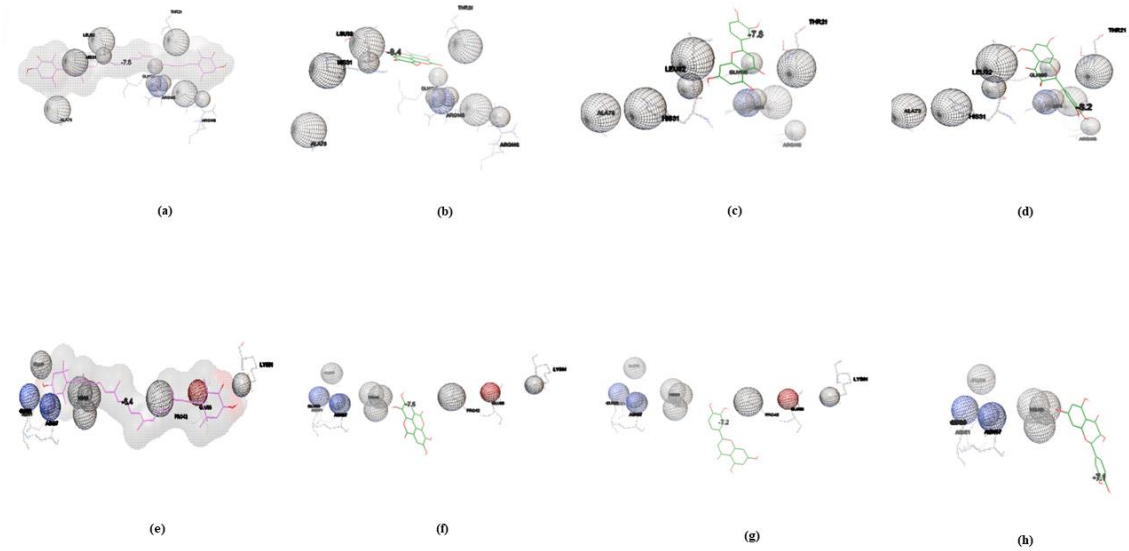

Figure 44. Affinity of SKR proteins: (i) 1L60 for **(a)** Astaxanthin, **(b)** Ellagic acid, **(c)** Luteolin, **(d)** Taxifolin, and (ii) 1WBU for **(e)** Astaxanthin, **(f)** Ellagic acid, **(g)** Luteolin, **(h)** Taxifolin.

Table 10 represents the binding energy or affinity values of 14 chosen proteins of kinases for 4 different ligands, namely Astaxanthin, ellagic acid, Luteolin, and Taxifolin. For Astaxanthin, protein 4X21 of kinase JNK showed a high affinity with an affinity score of -8.9 kcal/mol. Protein 4KIK of kinase IκBα showed high affinity for ellagic acid, Luteolin, and Taxifolin with an affinity score of -9.3 kcal/mol, -10.0 kcal/mol, and -9.3 kcal/mol, respectively.

The bar graph in Figure 45 represents the affinity score comparison of Astaxanthin, ellagic acid, Luteolin, and Taxifolin. It is clear that in some cases, the proteins showed greater affinity for ellagic acid or Astaxanthin or for both Astaxanthin and ellagic acid than the standard drugs, i.e., Luteolin and Taxifolin but in some instances, the proteins bound slightly better to the standard drugs. The proteins 4X21, 5MRD, and 1ZC0 showed better affinity towards Astaxanthin and ellagic acid and the standard drugs. The proteins 3O2M and 4X21 showed equal affinity for Astaxanthin and ellagic acid. The proteins 7MGJ, 5MRD, and 5G55 showed greater affinity towards Astaxanthin and ellagic acid. The proteins 5TCO, 4KIK, 5SFD, 1ZRZ, 1ZC0, 3VP4, 3LYM, 1L60, and 1WBU showed better affinity for ellagic acid than Astaxanthin. This clearly depicts the efficiency of ellagic acid as an inhibitor of the UV-mediated skin carcinogenesis pathway.

The bar graph in Figure 45 shows that the proteins 4X21,5MRD,1ZC0,3LYM showed drastically higher affinity for Astaxanthin and ellagic acid than the standard drug taxifolin, and the protein 7MGJ showed slightly higher affinity for Astaxanthin and ellagic acid than the standard drug taxifolin.

The bar graphs (Figure 45) demonstrated that ellagic acid has a higher affinity than Astaxanthin in binding to protein kinases such as JNK, IκBα, ERK1/2, and SKR. These findings suggest that both astaxanthin and ellagic acid act as potential inhibitors of kinases in the UV-induced skin cancer pathway. The efficiency of Astaxanthin and ellagic is higher than the standard drug taxifolin in most cases, and in certain cases, it is higher than Luteolin.

Table 9. Binding energy comparison.

Protein Kinase Targets	PDB ID of Proteins	Affinity scores/ Binding energy in kcal/mol				
		Astaxanthin	Ellagic Acid	Luteolin	Taxifolin	Average
JNK	3O2M	-8.4	-8.4	-9.0	-8.6	-8.4
	4X21	-8.9	-8.9	-8.0	-8.0	-8.9
P38	5TCO	-7.5	-8.8	-8.9	-8.7	-8.2
	7MGJ	-7.6	-7.5	-7.9	-7.5	-7.6
IκBα	4KIK	-8.1	-9.3	-10.0	-9.3	-8.7
	5SFD	-8.6	-9.1	-8.8	-9.0	-8.9
DNA-PKcs	1ZRZ	-7.0	-8.0	-8.2	-8.0	-7.5
	5MRD	-7.3	-6.3	-6.1	-5.8	-6.8
ERK 1/2	1ZC0	-6.4	-7.6	-6.2	-5.9	-7.0
	3VP4	-7.4	-8.3	-8.6	-8.0	-7.9
ATM	3LYM	-7.1	-8.0	-7.4	-7.3	-7.6
	5G55	-6.0	-5.5	-6.1	-5.9	-5.8
SKR	1L60	-7.5	-8.4	-7.8	-8.2	-8.0
	1WBU	-6.4	-7.5	-7.2	-7.1	-7.0

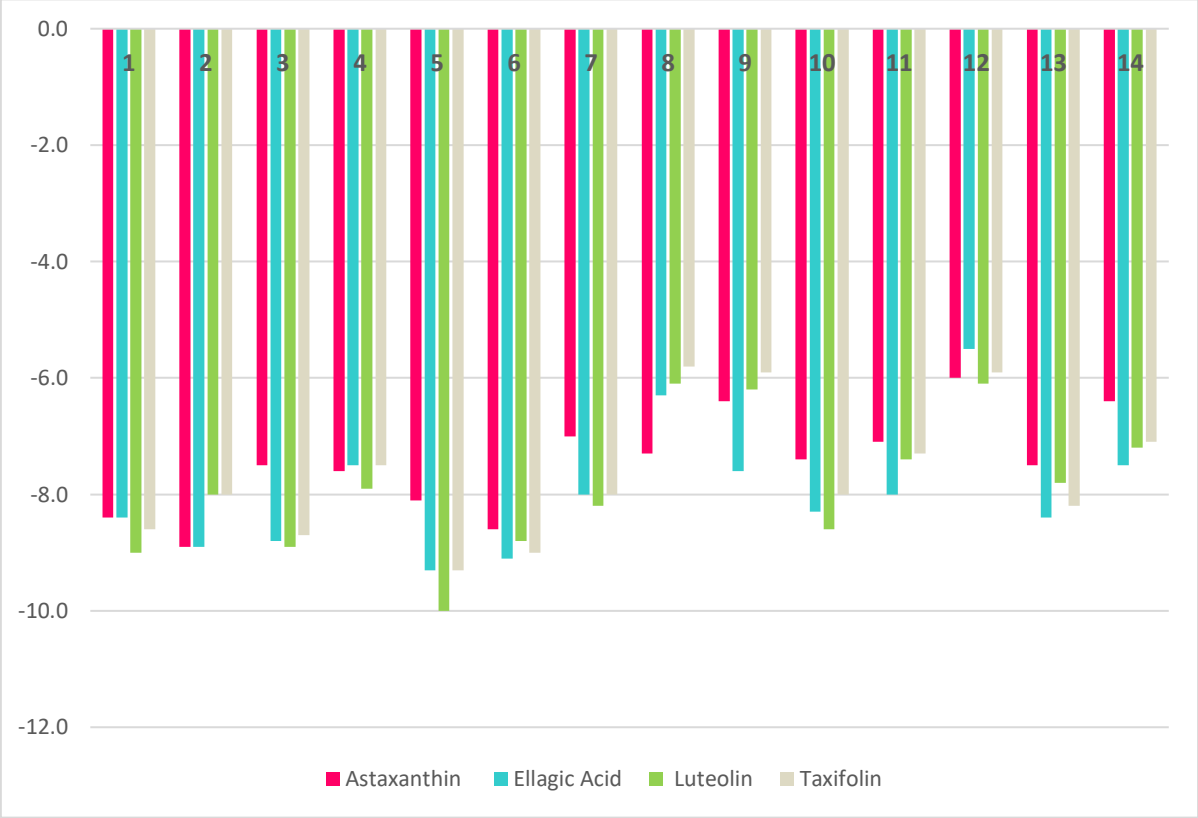

Figure 45. Binding energy comparison of Astaxanthin and Ellagic acid with standard drugs such as Luteolin and Taxifolin.

3.4. Inhibition Constant (Ki).

The inhibition constant (Ki) can be calculated from the binding energies from Table 4 using the following formula.

$$Ki = \exp(\Delta G \times 1000) / (R \times T)$$

where ΔG is the binding energy in kcal/mol, R is the universal gas constant in cal/K·mol, and T is the room temperature in kelvin. Here, R is 1.98719 cal/K·mol, and T is 298.15 K.

Table 11 shows the inhibition constants of Astaxanthin, ellagic acid, Luteolin, and Taxifolin. Figures 46(a)-(d) represent the relationship between the Inhibition constant (Ki) and Binding energies of 14 chosen proteins with Astaxanthin, ellagic acid, Luteolin, and Taxifolin., Figure 46 (e) shows that the relationship between binding energies and inhibition constant (Ki) is almost similar for all 14 proteins of 7 different protein kinases.

Table 10. Inhibition constant (Ki) comparison.

Protein Kinase Targets	PDB ID of Proteins	Inhibition constant (Ki) in μM				
		Astaxanthin	Ellagic Acid	Luteolin	Taxifolin	Average
JNK	3O2M	0.66	0.66	0.24	0.47	0.66
	4X21	0.28	0.28	1.30	1.30	0.28
P38	5TCO	3.04	0.34	0.28	0.40	1.01
	7MGJ	2.56	3.04	1.54	3.04	2.79
IκBα	4KIK	1.10	0.14	0.04	0.14	0.40
	5SFD	0.47	0.20	0.34	0.24	0.31
DNA-PKcs	1ZRZ	7.08	1.30	0.93	1.30	3.04
	5MRD	4.26	23.19	32.54	54.09	9.94
ERK 1/2	1ZC0	19.57	2.56	27.47	45.66	7.08
	3VP4	3.60	0.78	0.47	1.30	1.68

Protein Kinase Targets	PDB ID of Proteins	Inhibition constant (Ki) in µM				
		Astaxanthin	Ellagic Acid	Luteolin	Taxifolin	Average
ATM	3LYM	5.98	1.30	3.60	4.26	2.79
	5G55	38.54	89.91	32.54	45.66	58.87
SKR	1L60	3.04	0.66	1.83	0.93	1.42
	1WBU	19.57	3.04	5.05	5.98	7.71

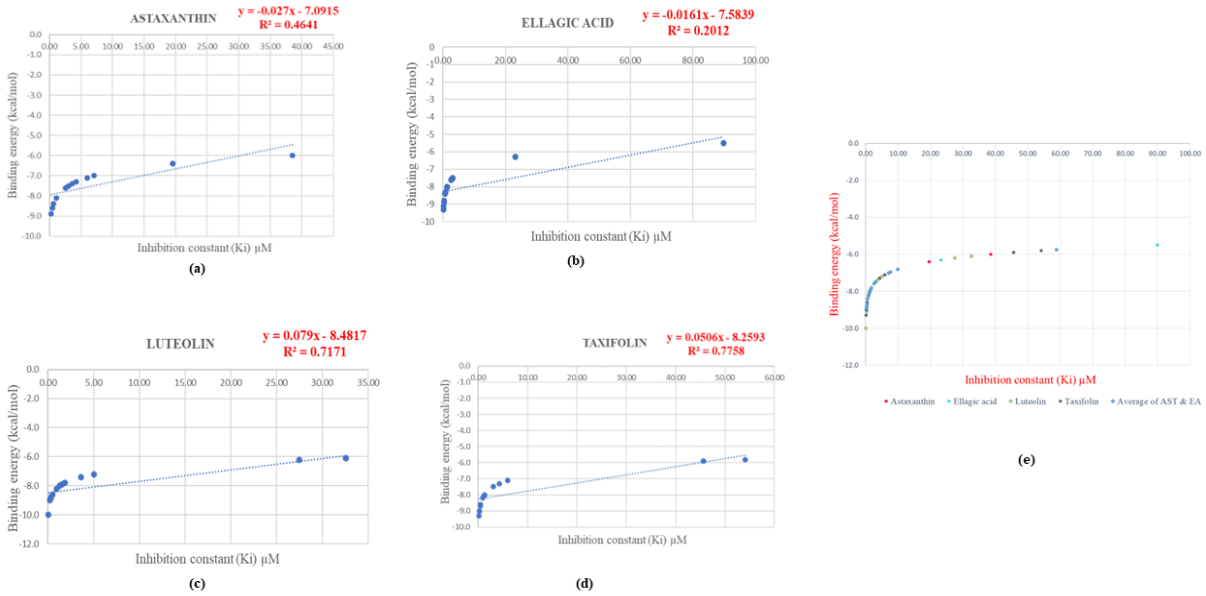

Figure 46. Relationship between Inhibition constant (Ki) and Binding energies of 14 chosen proteins with **(a)** Astaxanthin, **(b)** Ellagic acid, **(c)** Luteolin, and **(d)** Taxifolin. And **(e)** represents a comparison of the relationship between Inhibition constant (Ki) and Binding energies for Astaxanthin, Ellagic acid, Luteolin, and Taxifolin.

4. Conclusions

The potential of Astaxanthin and ellagic acid as inhibitors for UV-mediated skin carcinogenesis is confirmed through this *silico* study involving seven protein kinases. By comparing binding affinity, H-bonds, and inhibition constant (Ki) it is clear that astaxanthin and ellagic acid have almost similar efficiency against protein kinases than the standard drugs, i.e., Luteolin and Taxifolin. Astaxanthin and ellagic acid perform even better than the standard drugs against kinases JNK and DNA-PKcs.

Funding

This research received no external funding.

Acknowledgments

We thank the HoD, faculties, and supporting staff of the Department of Biotechnology, Kumaraguru College of Technology, Coimbatore-641049, for their constant support and encouragement.

Conflicts of Interest

The authors declare no conflict of interest.

References

1. Pfeifer, G.P. Mechanisms of UV-induced mutations and skin cancer. *Genome Instab. Dis.* **2020**, *1*, 99–113, https://doi.org/10.1007/S42764-020-00009-8.
2. Kim, M.J.; Ha, S.J.; So, B.R.; Kim, C.K.; Kim, K.M.; Jung, S.K. Nadph oxidase and epidermal growth factor receptor are promising targets of phytochemicals for ultraviolet-induced skin carcinogenesis. *Antioxidants* **2021**, *10*, https://doi.org/10.3390/antiox10121909.
3. Hein, A.L.; Ouellette, M.M.; Yan, Y. Radiation-induced signaling pathways that promote cancer cell survival (Review). *Int. J. Oncol.* **2014**, *45*, 1813–1819, https://doi.org/10.3892/ijo.2014.2614
4. Emri, G.; Paragh, G.; Tósaki, Á.; Janka, E.; Kollár, S.; Hegedűs, C.; Gellén, E.; Horkay, I.; Koncz, G.; Remenyik, É. Ultraviolet radiation-mediated development of cutaneous melanoma: An update. *J. Photochem. Photobiol. B Biol.* **2018**, *185*, 169–175, https://doi.org/10.1016/j.jphotobiol.2018.06.005.
5. Sugiura, R.; Satoh, R.; Takasaki, T. ERK: A Double-Edged Sword in Cancer. ERK-Dependent Apoptosis as a Potential Therapeutic Strategy for Cancer. *Cells* **2021**, *10*, https://doi.org/10.3390/cells10102509.
6. López-Camarillo, C.; Aréchaga Ocampo, E.; López Casamichana, M.; Pérez-Plasencia, C.; Álvarez-Sánchez, E.; Marchat, L.A. Protein Kinases and Transcription Factors Activation in Response to UV-Radiation of Skin: Implications for Carcinogenesis. *Int. J. Mol. Sci.* **2012**, *13*, 142–172, https://doi.org/10.3390/ijms13010142.
7. Suganya, V.; Anuradha, V. In silico molecular docking of Astaxanthin and sorafenib with different apoptotic proteins involved in hepatocellular carcinoma. *Biocatal. Agric. Biotechnol.* **2019**, *19*, 101076, https://doi.org/10.1016/J.BCAB.2019.101076.
8. Lin, Z.; Li, F.; Zhang, Y.; Tan, X.; Luo, P.; Liu, H. Analysis of astaxanthin molecular targets based on network pharmacological strategies. *J. Food Biochem.* **2021**, *45*, https://doi.org/10.1111/JFBC.13717.
9. Chung, B.Y.; Park, S.H.; Yun, S.Y.; Yu, D.S.; Lee, Y.B. Astaxanthin Protects Ultraviolet B-Induced Oxidative Stress and Apoptosis in Human Keratinocytes via Intrinsic Apoptotic Pathway. *Ann. Dermatol.* **2022**, *34*, 125, https://doi.org/10.5021/AD.2022.34.2.125.
10. Yang, H.L.; Lin, C.P.; Vudhya Gowrisankar, Y.; Huang, P.J.; Chang, W.L.; Shrestha, S.; Hseu, Y.C. The anti-melanogenic effects of ellagic acid through induction of autophagy in melanocytes and suppression of UVA-activated α-MSH pathways via Nrf2 activation in keratinocytes. *Biochem. Pharmacol.* **2021**, *185*, https://doi.org/10.1016/j.bcp.2021.114454.
11. Ortiz-Ruiz, C.V.; Berna, J.; Tudela, J.; Varon, R.; Garcia-Canovas, F. Action of ellagic acid on the melanin biosynthesis pathway. *J. Dermatol. Sci.* **2016**, *82*, 115–122, https://doi.org/10.1016/j.jdermsci.2016.02.004.
12. Dahiya, R.; Mohammad, T.; Gupta, P.; Haque, A.; Alajmi, M.F.; Hussain, A.; Hassan, M.I. Molecular interaction studies on ellagic acid for its anticancer potential targeting pyruvate dehydrogenase kinase 3. *RSC Adv.* **2019**, *9*, 23302–23315, https://doi.org/10.1039/C9RA02864A.
13. Cheshomi, H.; Bahrami, A.R.; Matin, M.M. Ellagic acid and human cancers: a systems pharmacology and docking study to identify principal hub genes and main mechanisms of action. *Mol. Divers.* **2021**, *25*, 333–349, https://doi.org/10.1007/S11030-020-10101-6.
14. Juszczak, A.M.; Wöelfle, U.; Marijana, |; Končić, Z.; Tomczyk, M. Skin cancer, including related pathways and therapy and the role of luteolin derivatives as potential therapeutics. *Wiley Online Libr.* **2022**, *42*, 1423–1462, https://doi.org/10.1002/med.21880.
15. Gendrisch, F.; Esser, P.R.; Schempp, C.M.; Wölfle, U. Luteolin as a modulator of skin aging and inflammation. *BioFactors* **2021**, *47*, 170–180, https://doi.org/10.1002/BIOF.1699.
16. Caporali, S.; De Stefano, A.; Calabrese, C.; Giovannelli, A.; Pieri, M.; Savini, I.; Tesauro, M.; Bernardini, S.; Minieri, M.; Terrinoni, A. Anti-Inflammatory and Active Biological Properties of the Plant-Derived Bioactive Compounds Luteolin and Luteolin 7-Glucoside. *Nutrients* **2022**, *14*, 1–19, https://doi.org/10.3390/nu14061155.
17. Thuan, N.H.; Shrestha, A.; Trung, N.T.; Tatipamula, V.B.; Van Cuong, D.; Canh, N.X.; Van Giang, N.; Kim, T.S.; Sohng, J.K.; Dhakal, D. Advances in biochemistry and the biotechnological production of Taxifolin and its derivatives. *Biotechnol. Appl. Biochem.* **2022**, *69*, 848–861, https://doi.org/10.1002/BAB.2156.
18. Das, A.; Baidya, R.; Chakraborty, T.; Samanta, A.K.; Roy, S. Pharmacological basis and new insights of Taxifolin: A comprehensive review. *Biomed. Pharmacother.* **2021**, *142*, https://doi.org/10.1016/j.biopha.2021.112004.
19. Wang, R.; Zhu, X.; Wang, Q.; Li, X.; Wang, E.; Zhao, Q.; Wang, Q.; Cao, H. The antitumor effect of

Taxifolin on lung cancer via suppressing stemness and epithelial-mesenchymal transition in vitro and oncogenesis in nude mice. *Ann. Transl. Med.* **2020**, *8*, 590–590, https://doi.org/10.21037/ATM-20-3329.
20. Oi, N.; Chen, H.; Kim, M.O.; Lubet, R.A.; Bode, A.M.; Dong, Z. Taxifolin suppresses UV-induced skin carcinogenesis by targeting EGFR and PI3-K. *Cancer Prev. Res. (Phila).* **2012**, *5*, 1103, https://doi.org/10.1158/1940-6207.CAPR-11-0397.
21. Aras, M.; Yayintaş, Ö.T. In silico analysis of quercetin, gallic acid, oleanolic acid, and ursolic acid on diabetes mellitus. *Troia Med. J.* **2022**, *3*, 100–110, https://doi.org/10.55665/TROIAMEDJ.1163784.
22. Tian, W.; Chen, C.; Lei, X.; Zhao, J.; Liang, J. CASTp 3.0: Computed atlas of surface topography of proteins. *Nucleic Acids Res.* **2018**, *46*, W363–W367, https://doi.org/10.1093/nar/gky473.
23. Eissa, I.H.; Ibrahim, M.K.; Alesawy, M.S.; El-Adl, K. Antiproliferative evaluations of triazoloquinazolines as classical DNA intercalators: Design, synthesis, ADMET profile, and molecular docking. *Arch. Pharm. (Weinheim).* **2022**, *355*, https://doi.org/10.1002/ARDP.202100487.
24. Atiya, A.; Alsayari, A.; Bin Muhsinah, A.; Almaghaslah, D.; Bilgrami, A.L.; Abdulmonem, W. Al; Alorfi, N.M.; DasGupta, D.; Ashraf, G.M.; Shamsi, A.; et al. Role of lisinopril in the therapeutic management of cardiovascular disease by targeting microtubule affinity regulating kinase 4: molecular docking and molecular dynamics simulation approaches. *J. Biomol. Struct. Dyn.* **2022**, https://doi.org/10.1080/07391102.2022.2143425.
25. Ismail, S.; Waheed, Y.; Ahmad, S.; Ahsan, O.; Abbasi, S.W.; Sadia, K. An in silico study to unveil potential drugs and vaccine chimera for HBV capsid assembly protein: combined molecular docking and dynamics simulation approach. *J. Mol. Model.* **2022**, *28*, https://doi.org/10.1007/S00894-022-05042-W.